INT. J. REMOTE SENSING, 1994, VOL. 15, NO. 12, 2437-2450

Identifying spatial patterns of Mediterranean landscapes from geostatistical analysis of remotely-sensed data

B. LACAZE, S. RAMBAL and T. WINKEL†

Centre d'Ecologie Fonctionnelle et Evolutive, Centre National de la Recherche Scientifique, B.P. 5051, 34033 Montpellier Cedex 1, France

Abstract. The basic tool of geostatistics, the semi-variogram, has been used for quantifying spatial structures of soil and vegetation, as depicted by multi-resolution remotely-sensed images. Experimental semi-variograms of two contrasting Mediterranean landscapes were analysed by reference to simple theoretical models (spherical, exponential, allometric). A more general approach based on the superposition of spherical models of similar sills and varying ranges of influences is proposed for the interpretation of complex spatial patterns of natural vegetated landscapes.

1. Introduction

Remote sensing offers efficient possibilities of characterizing the structure of terrestrial ecosystems (Graetz 1990) and can yield correlative assessments of functional features such as primary productivity, up to large scales. For many years, a lot of time and effort have been devoted to quantitative analysis of spectral information but the extraction of information from the spatial domain has been considerably less developed because of the lack of understanding of spatial variations in the imagery.

Recently some authors suggested making use of geostatistical analysis using a set of techniques based upon the theory of regionalized variables (Matheron 1965). Geostatistics have been applied to remotely-sensed data in the form of the semi-variogram, a basic tool (Curran 1988, Ramstein and Raffy 1989, Woodcock *et al.* 1988, Cohen *et al.* 1990).

Another approach has been taken from fractal geometry (Mandelbrot 1975), which implies invariance of probability distributions with respect to changes of scale (self-similarity) and provides an economical framework for the representation of the spatial properties of landscapes which are visible in remote sensing imagery (DeCola 1989, Jones *et al.* 1991). Various links can be established between fractal geometry and geostatistics (Burrough 1983): for example, the fractal dimension of a spatialized variable can be deduced from its variogram.

The techniques used in this paper are borrowed from geostatistics and are illustrated by two applications taken from a Mediterranean environment, the first being an agricultural landscape dominated by vineyards and the second a naturally vegetated landscape. We intend to demonstrate the possibilities of identifying multiscale spatial patterns from the analysis of remotely-sensed data and to suggest an interpretation of these patterns in the two cases studied.

†Present address: ORSTOM, B.P. 11416, Niamey, Niger.

0143-1161/94 $10.00

2. Methods

2.1. *Variography*

The key to geostatistics is the semi-variogram, which is a graphical representation of the spatial variability in a given set of data. Structural analysis of spatial dependence using semi-variograms can be made using weaker assumptions of stationarity than are necessary for autocorrelation (Trangmar *et al.* 1985). The basic assumption is that the difference in value of a regionalized variable observed at two positions depends only on the distance between sampled points and their orientation. Semi-variance $\gamma(h)$ is defined as half the expected squared difference between sample values Z separated by a given lag (or distance) h, i.e.:

$$2\gamma(h) = E[Z(x_i) - Z(x_i + h)]^2 \tag{1}$$

The semi-variance at a given lag h is estimated as the average of the squared differences between all observations separated by the lag:

$$\gamma^*(h) = \frac{1}{2N(h)} \sum_{i=1}^{N(h)} [Z(x_i) - Z(x_i + h)]^2 \tag{2}$$

where $N(h)$ is the number of pairs of observations at lag h. At least 80 to 100 pairs are necessary for each estimate (Webster 1985). The semi-variogram is usually displayed as a plot of semi-variance against distance. The shape of a semi-variogram may take many forms, which can be related to several models:

(1) The spherical model:

$$\gamma(h) = c\left(\frac{3}{2}\frac{h}{a} - \frac{1}{2}\frac{h^3}{a^3}\right) \quad \text{when} \quad h \leqslant a \tag{3}$$

$$\gamma(h) = c \quad \text{when} \quad h \geqslant a$$

In this commonly used model, the semi-variance rise to a more or less constant value (the sill c) after a given range a. The point where the extrapolated relationship $\gamma(h)/h$ intercepts the (h) axis is not always the origin: in some case there may exist a spatially independent variance (nugget variance).

(2) The exponential model:

$$\gamma(h) = c[1 - e^{(-h/r)}] \tag{4}$$

where c is the sill, and r is a distance parameter controlling the spatial extent of the function. The exponential model can be considered as 'the essence of randomness in space' (Webster 1985) and represents the variogram of first-order auto-regressive processes.

These first two models are often referred to as authorized models in geostatistics. Other models correspond to unbounded semi-variograms, i.e., without sill:

1. The linear model:

$$\gamma(h) = p^h \tag{5}$$

semi-variance is regularly increasing with distance.

2. The allometric or power function model:

$$\gamma(h) = ph^{\alpha} \tag{6}$$

it is a generalization of the linear model; there is a linear relationship between $\mathrm{Log}\,\gamma(h)$ and $\mathrm{Log}\,h$.

3. The de Wijs's model:

$$\gamma(h) = 3\alpha\,\mathrm{Log}\,h \tag{7}$$

there is a linear relationship between $\gamma(h)$ and $\mathrm{Log}\,h$.

Experimental semi-variograms can be obtained from remotely-sensed images by examining the spatial variation of radiances along transects (mono-dimensional case), or by considering all directions (bi-dimensional case). In this study we used mono-dimensional semi-variograms computed from lines of pixels along four directions in the images: 0°, 45°, 90° and 135° from the scan direction, referred to as west-east, south-west-north-east, south-north and south-east-north-west directions. For each considered direction a mean semi-variogram has been computed from all available lines in the studied part of the image. Some experimental semi-variograms have been fitted to theoretical models: the parameters were estimated using least-squares regression, weighted for the number of sample pairs at each lag (Cressie 1985).

2.2. *Fractal geometry*

An object is considered as fractal if the Hausdorff-Besicovitch dimension D exceeds the Euclidean dimension (Mandelbrot 1975). This is the case for objects exhibiting structural details at all scales, for example outlines of clouds or plant communities (Palmer 1988). Fractal geometry allows dimensions between 1 (strict spatial dependence) and 2 (complete spatial independence) for a line and between 2 and 3 for a surface.

One approach to fractal dimension estimation is based on the allometric model of the variogram (Burrough 1983):

$$\gamma(h) = h^{2H} \tag{8}$$

H is a scale factor related with fractal dimension; $D = 2 - H$ (monodimensional case), or $D = 3 - H$ (bidimensional case). Consequently, if we consider the slope m of the double logarithmic variogram, the fractal dimension is given by $D = (4 - m)/2$ in the monodimensional case and $D = (6 - m)/2$ in the bidimensional case.

3. Multi-scale spatial patterns in a vineyard landscape

3.1. *Description of the study area and data collection*

The studied area is located in the Aude Valley of Southern France at 43°13 N, 2°50 E, in a region of Mediterranean climate. Its potential evaporation rate is about 1100 mm y^{-1}, and its mean annual rainfall is about 600 mm. The vineyard plot selected for intensive ground measurements stands on a nearly level Quaternary terrace (Würm) between the Aude and the Orbieu rivers. Its brown calcareous soil consists of a silty clay to silty clay loam topsoil covering a discontinuous gravel layer that is more or less hard. This discontinuous layer represents the main source of soil variation in the vineyard. The vineyard was uniformly planted and the six-year-old vines were of a single cultivar (Shiraz grafted on R110), cordon trained with 1·5 m between plants along the rows, which ran from west to east. Tillage as well as pest and weed control were the same throughout. The vines had received no irrigation since planting.

A transection, 300 m long, was laid across the whole vineyard, parallel to the rows of vines in the west-east direction. Soil and plants were measured at equispaced points at intervals that depended on the studied property.

The total dry shoot biomass per vine, which is a function of the cumulative transpiration (Mériaux *et al.* 1979), provided an index of plant cover. The biomass of the shoot was measured on each vine of the transection, i.e., at an interval of 1·5 m, omitting the recently substituted vines. The biomass measured on 3 February 1988 represents the annual shoot production per vine for 1987.

Soil particle size distribution (clay: $<2\,\mu$m; fine silt: 2–10 μm; coarse silt: 10–20 μm; fine sand: 20–200 μm; coarse sand: 0·2–2 mm) and the gravel percentage (>2 mm) were determined for 61 soil surface samples taken along the transection at 6 m intervals. Cultivation had mixed the soil to a depth of 40 to 60 cm, and so these samples represent a deep topsoil. The soil was sampled between two rows of vines (viz. 1 m from the vines) and sieved through a 10 mm sieve to remove clods and large stones. The soil samples were sieved again in the laboratory at 2 mm and the coarse fraction (2–20 mm) expressed as a proportion by weight. The particle size distribution of sand, silt and clay, was determined by sieving and pipette analysis. The samples were analysed in random order to avoid systematic errors within the series.

Bare soil reflectance was measured on 29 July 1987, along the same transection. The soil surface was dry, without weeds and had been tilled 2 days before, so surface rugosity was roughly similar along the transection. Reflectance measurements were recorded with a SPOT simulation, hand-held radiometer (Cimel Electronique), working in three channels: green (0·50 to 0·59 μm), red (0·61 to 0·68 μm) and near-infrared (0·79 to 0·89 μm). The radiometer was held at 1·5 m above soil level, measuring outcoming radiation from a circular surface of about 0·08 m^2. Measurements were made at 3 m intervals along the transection.

The same 300 m transection has been analysed with data sampled from an aerial photograph taken in September 1986 at the scale of 1/17 500. This colour infrared photograph has been digitized using colour filters in order to simulate 3-band measurements (green, red and near-infrared) with 5 m spatial resolution.

With a view to analysing a larger area of this agricultural landscape, data were extracted from colour infrared aerial photographs and available satellite images. The chosen area is a rectangle of about 2 km by 1·25 km, located on the flood plain at approximately 1·6 km from the Aude river. The landscape is highly dominated by vineyards and appears as a mosaic of cultivated plots, varying in size from 0·1 to 2·5 ha. Remote sensing measurements were selected from digitized colour infrared photographs (September 1986), from a SPOT scene recorded on 21 May 1987 (20 m spatial resolution) and from a Landsat Thematic Mapper scene recorded on 4 July 1984 (30 m resolution). The normalized difference vegetation index was generated from red and near-infrared (NIR) values as NDVI = (NIR − red)/(NIR + red).

3.2. *Results*

3.2.1. *Site level: the vineyard plot*

Statistical results (means and variances) obtained from ground measurements along the 300 m transection are given in table 1. With the exception of gravel (log-normal distribution) all measured variables can be adjusted to Gaussian distributions.

Table 1. Studied variables, means, variances and types of experimental semi-variograms for the vineyard transection.

Variable	Mean	Variance	Semi-variogram
Soil texture (‰):			
Total sand	182·9	847·1	spherical
Coarse sand	39·1	180·5	linear
Fine sand	143·8	394·4	spherical
Total silt	526·2	496·5	linear
Coarse silt	167·8	99·9	periodical
Fine silt	358·4	421·2	linear
Clay	290·9	164·3	periodical
Gravel	20·0	357·2	spherical
Soil reflectance			
Red channel (× 10)	195·6	83·6	periodical
NIR channel (× 10)	252·1	143·5	periodical
NDVI (× 1000)	126·1	118·9	spherical
Vegetation			
Plant cover index	399·4	11091·2	aspatial

Some experimental semi-variograms obtained from the same data are displayed in figure 1, which also shows semi-variograms generated from digitized aerial photography measurements.

These experimental semi-variograms are related to several types of theoretical models (see table 1):

(*a*) Aspatial: this is the case for plant cover index; no clear spatial structure is apparent and variance is rather high at the shortest lag (nugget effect related to a distance of 1·5 m between vine plants along the row).

(*b*) Unbounded: some soil texture parameters (coarse sand, fine silt,...) exhibit linear semi-variograms; the transection is not long enough to detect any specific spatial extent of these parameters.

(*c*) Spherical: for soil parameters such as total sand, fine sand, gravel percentage, the semi-variogram is spherical and the sill is reached for a range value of about 110 to 120 m. This characteristic scale can be related to the result of pedogenetic factors during the formation of the terrace.

(*d*) Periodic for coarse silt and clay, the main feature in the semi-variogram is the dip in the curve occurring at about 80 m, revealing the existence of a periodic phenomenon at this scale. This periodicity can be attributed to hydrodynamic flows during the alluvial phase of terrace formation, inducing deposition of well individualized interlacing benches with different silt and clay contents. Although recorded at different spatial resolutions, soil reflectances (measured by hand-held radiometry) and digitized photography data, exhibit the same periodicity effect in their semi-variograms. This means that soil reflectances vary with soil surface characteristics correlated with silt and clay content. This can be confirmed through the computation of cross-variograms: figure 2 gives the example of a cross-variogram between soil spectral hand-held measurements (NDVI) and silt content.

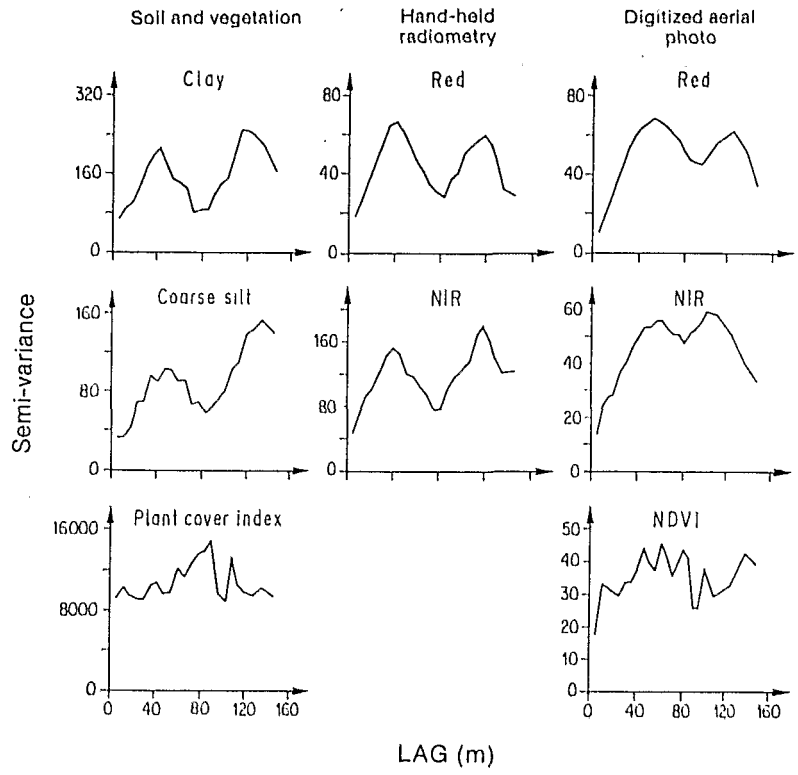

Figure 1. Experimental semi-variograms obtained at site level (vineyard plot).

Because of the low percentage of vegetation cover (20 per cent in September 1986) and of the high brightness of bare soil resulting from a period of severe drought (only 40 mm rainfall between May and September 1986) data from aerial photography are mainly influenced by soil surface characteristics. Another factor affecting the shape of the variogram is the regularization (Clark 1979, Woodcock *et al.* 1988) resulting from the change of spatial resolution (0.08 m^2 for hand-held

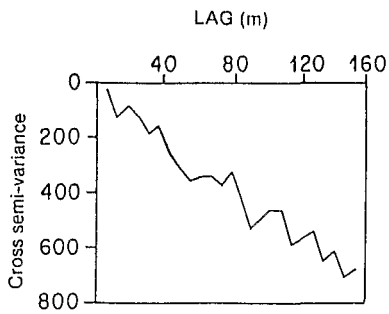

Figure 2. Experimental cross-variogram between soil spectral measurements (NDVI) and coarse silt content.

radiometry and 25 m^2 for digitized photography). Using NDVI values partly eliminates the periodic effect linked with soil properties, the semi-variogram then reflects more directly spatial patterning induced by vegetation and shadows.

3.2.2. *Landscape level*

Directional semi-variograms derived from aerial photography and satellite data (2 km by 1·25 km test area) are shown in figure 3. Only results from the west/east direction are given, semi-variograms obtained at three other directions being roughly similar.

All experimental semi-variograms exhibit a similar bounded shape with some differences at shortest lags resulting from the regularization effect (increased pixel size from 5 m to 30 m). The sill is reached at about 150 m in all directions. This can be linked with the mean size of agricultural fields in the studied area. In this artificial landscape, spatial structures at the local level result mainly from cultivation patterns.

In the thermal infrared channel (Landsat-TM), semi-variance remains rather low. The original spatial resolution of this channel is 120 m, a value close to the mean

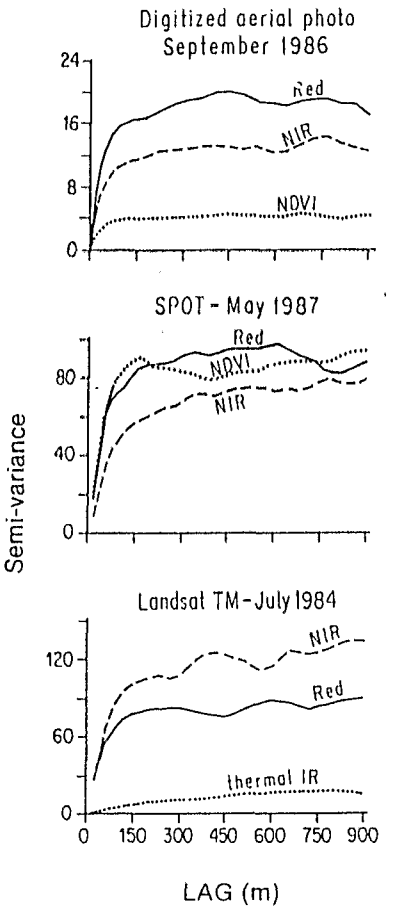

Figure 3. Experimental semi-variograms obtained at landscape level.

field size, however, the acquisition time of data (mid-morning) is not convenient for high thermal contrasts and specific spatial structures are not easy to identify in this channel.

4. Multi-scale spatial patterns in a natural vegetated landscape

4.1. *Description of the study area and data collection*

The test area is a small watershed (about 50 km^2) located 20 km north of Montpellier, France, and representative of Mediterranean karst watersheds. It was chosen because of its homogeneous lithologic substratum and the relative flatness of the terrain.

Vegetation cover is characterized by shrublands ('garrigue') and semi-dense to dense woodlands. Dominant tree species are the evergreen holm oak (*Quercus ilex* L.) and the deciduous downy oak (*Quercus pubescens* Willd.).

Satellite sensor data were obtained from the Heat Capacity Mapping Mission (HCMM) of the Explorer I satellite (NASA 1980) and from SPOT multi-spectral data. HCMM spectral radiances in visible/near-infrared and thermal infrared channels were recorded with a spatial resolution of 500 m by 500 m. Five acquisition dates were considered: 6 May, 4 July, 21 and 31 August and the 27 September 1979. Only diurnal data, obtained close to the daytime maximum, have been taken into account. Albedo values were derived from the calibration equation provided by NASA (1980). To reduce the effect of atmospheric variations between the five dates, we adopted a normalization procedure, assigning an albedo value recorded over seawater of 0·05, a value considered as relatively constant in the literature. The derived albedo values, which are more precisely spectral albedos measured in the 0·55 to 1·1 μm domain, are comparable to literature values, other satellite estimates and ground measurements (Lacaze *et al.* 1984, Rambal *et al.* 1990). In a similar way, surface temperatures were computed with the calibration equations published by NASA (1980), modified by the linear correction proposed by Reiniger (1981).

SPOT data were extracted from a scene recorded on 1 May 1986. In addition, data from an airborne SPOT simulation (10 m spatial resolution in 3 channels) concerning a 7 km transection in a similar landscape (cf. Lacaze *et al.* 1985) were considered.

4.2. *Results*

4.2.1. *Low resolution data*

Experimental semi-variograms for spectral albedo and surface temperature derived from HCMM data obtained on the 5 dates considered are given in figure 4. Semi-variances were calculated for the first 11 lags only in order to ensure a minimum of 80 data pairs. The results displayed in figure 3 are mean semi-variograms obtained from two directions (north-south and east-west).

Semi-variances are highest during the spring period, which is the phenological period of deciduous foliage growth. There is an apparent homogenization of albedos and surface temperatures during the summer period of increasing water stress.

The main feature of the multitemporal analysis is the similarity of the curves of the semi-variograms for the five dates. Albedo semi-variograms can be related to a spherical model, the sill being reached at a range of influence of about 3 to 4 km for

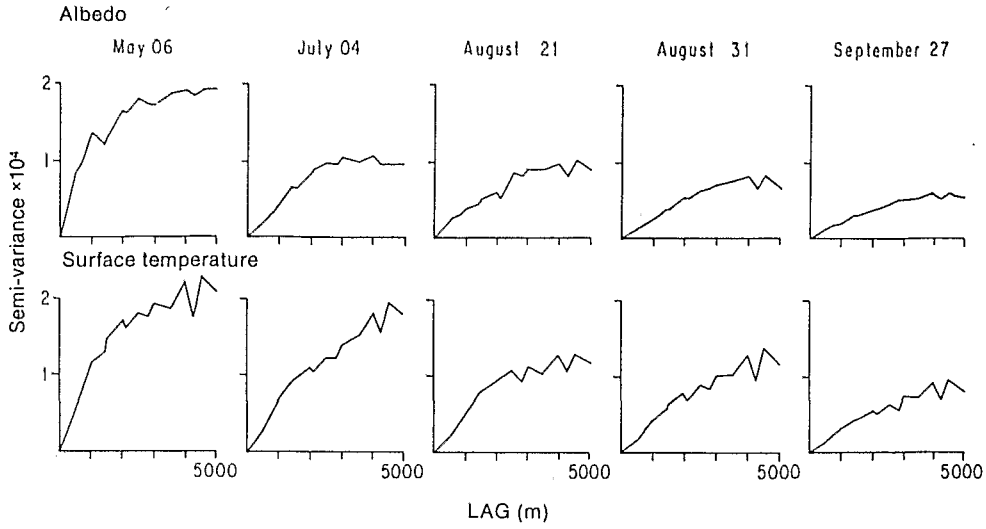

Figure 4. Experimental semi-variograms obtained from multi-temporal HCMM data for naturally vegetated landscape.

Table 2. Parameters of the spherical models fitted on the experimental semi-variograms of albedo for the five dates.

Date	Range (m)	Sill × 10^{-4}	Variance of raw data × 10^{-4}
6 May	4100	2·20	1·82
4 July	2900	0·99	0·96
21 August	4000	0·79	0·68
31 August	3800	0·73	0·66
27 September	4200	0·59	0·50

all dates (table 2). Surface temperature semi-variograms can be related to an exponential model: semi-variance rises more slowly from the origin and the sill is not reached at the longest lag (table 3). A presentation of the results is given in figures 5 and 6, where the mean semi-variograms for the five dates, normalized by the maximum sill, are displayed, such that spatial structures of albedo and surface temperature parameters appear different but persistent through time.

Semi-variogram were also used for deriving fractal dimension by plotting $Ln[\gamma(h)] = f(Ln\,h)$ close to the origin (Burrough 1983). Considering the five dates in question the derived fractal dimensions are 2·81, 2·63, 2·75, 2·59 and 2·66, and for surface temperature 2·72, 2·61, 2·64, 2·58 and 2·62. The mean fractal dimension of surface temperature (2·63) appears lower than the value obtained for albedo (2·69) which suggests a slight homogenization of surface temperatures of neighbouring pixels as was already noticeable from the shape of the semi-variograms.

Fractal dimensions of remotely-sensed parameters can be compared to values related to altitude and vegetation units as depicted by a physiognomic map, analysed

Table 3. Parameters of the exponential models fitted on the experimental semi-variograms of surface temperature for the five dates in question.

Date	Distance parameter (m)	Sill ($°C^2$)	Variance of raw data ($°C^2$)
6 May	1850	2·40	2·20
4 July	5200	3·20	1·73
21 August	1150	1·10	1·22
31 August	2300	1·50	1·14
27 September	2700	1·00	0·83

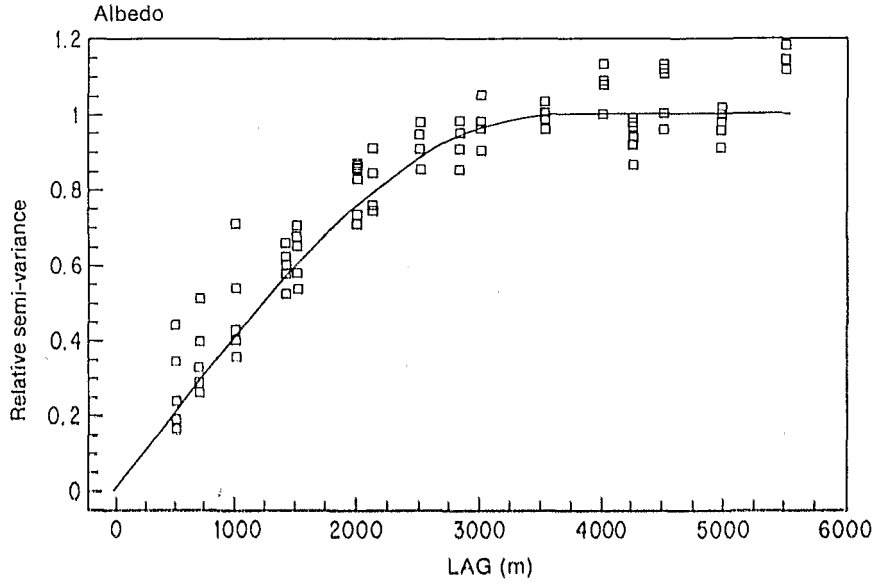

Figure 5. Normalized mean semi-variogram obtained from HCMM data for albedo (spherical model = solid line).

at the same spatial resolution of 500 m. Fractal dimensions of altitude and vegetation cover are 2·51 and 2·69 respectively. It is worthwhile to note the concordance between the fractal dimensions of albedo and vegetation, which corroborates the close links between vegetation cover and spectral measurements in the visible/near-infrared wavelengths.

4.2.1. *High resolution data*

Figure 7 presents results from SPOT data (NDVI), showing directional semi-variograms and the mean of four directions.

These results indicate an anisotropic effect. The curves of the semi-variograms are different for directions south-west–north-east and south–north (unbounded) and for the other two directions (bounded). The mean semi-variogram thus appears

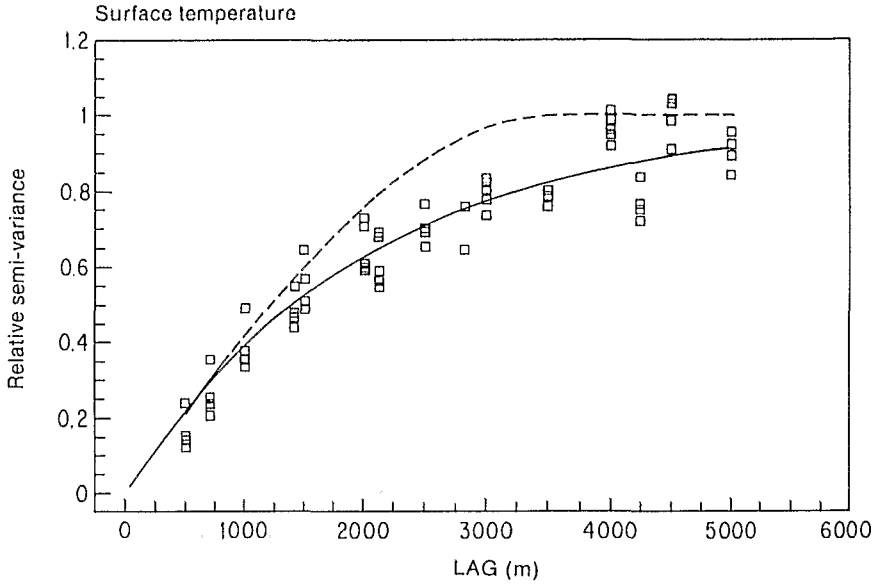

Figure 6. Normalized mean semivariograms obtained from HCMM data for surface temperature (exponential model = solid line); for comparison the spherical model of albedo is indicated (dashed line).

more irregular than those obtained from HCMM data suggesting a more complex interpretation. As in many practical cases one can consider that an experimental semi-variogram is a mixture of two or more theoretical models (Clark 1979).

This hypothesis of superposition of models has been further tested using the results of airborne SPOT simulation data. Figure 8 shows the experimental semi-variogram for SPOT channel XS2. This semi-variogram can be approximated by a single allometric model but a best fit is obtained when considering a superposition of two spherical models, with respective sill values of 92 and 103 and range values of 60 m and 450 m, with a residual variance (nugget effect) of 75:

$$\gamma(h) = 75 + 92\left[\frac{3}{2}\times\frac{h}{60} - \frac{1}{2}\left(\frac{h}{60}\right)^3\right] + 103\left[\frac{3}{2}\times\frac{h}{450} - \frac{1}{2}\left(\frac{h}{450}\right)^3\right] \quad \text{when } h \leqslant 60\text{ m}$$

$$\gamma(h) = 167 + 103\left[\frac{3}{2}\times\frac{h}{450} - \frac{1}{2}\left(\frac{h}{450}\right)^3\right] \quad \text{when } 60 \leqslant h \leqslant 450\text{ m}$$

$$\gamma(h) = 270 \quad \text{when } h \geqslant 450\text{ m}$$

A formalization of the idea of superposition of spherical models has been given by Serra (1968). The superposition of a minimum of three spherical models of similar sills and ranges of influence varying in geometric progression leads to a de Wijsian model. Imagery of naturally vegetated areas often exhibit spatial variations inducing unbounded semi-variograms that are better described by a de Wijsian model than an allometric model (Lacaze unpublished data). It is therefore possible to propose an idealized geometric progression of spatial ranges of variables influencing remotely-sensed measurements from site to regional level (table 4). This hierarchical approach can be related to the level of integration concept used in

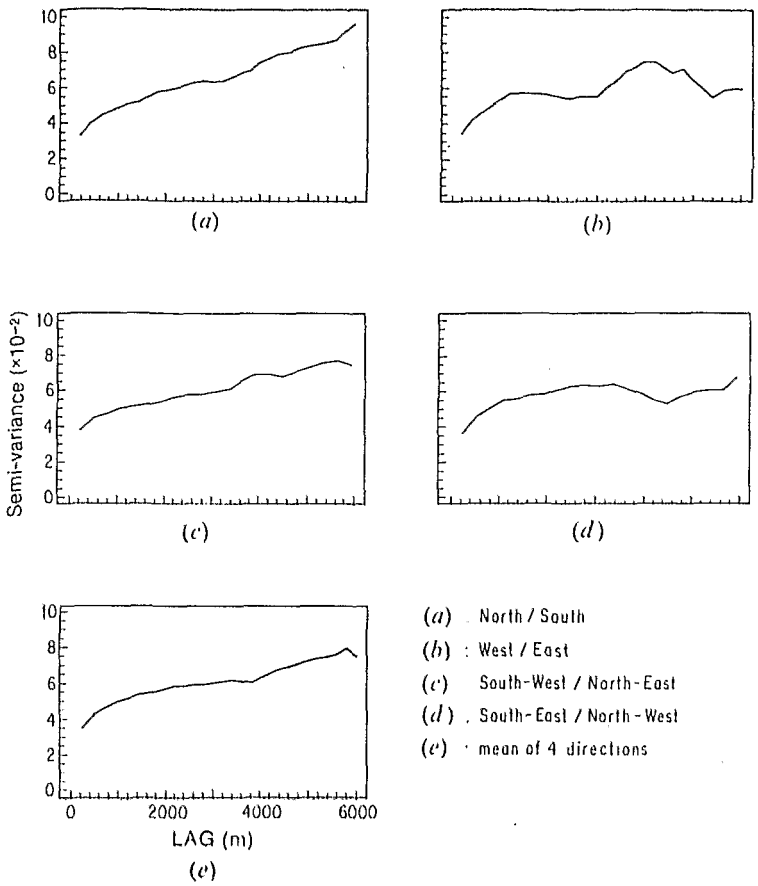

Figure 7. Directional semi-variograms derived from SPOT NDVI data (same test area as figures 5 and 6).

ecology (Rowe 1961) and gives a general framework for interpreting complex patterns of naturally vegetated areas.

5. Conclusion

The spatial patterns of two contrasting Mediterranean landscapes have been analysed by means of multi-resolution remote sensing data and quantified using semi-variograms.

In the first case study, spatial patterns of soil and cultivated vegetation have been compared. Small scale patterns of soil parameters have been detected, inducing different levels of water availability for the vegetation. These spatial variations are however buffered by the plants which are adapted to water stress through their deep rooting systems. From aerial photographs soil patterns can be identified at the site level. At the landscape level, field patterns become preponderant and can be detected from aerial photos and high resolution satellite data.

The second case study has been focused on multi-resolution and multi-temporal analysis of natural vegetation patterns. From low resolution satellite data, spatial

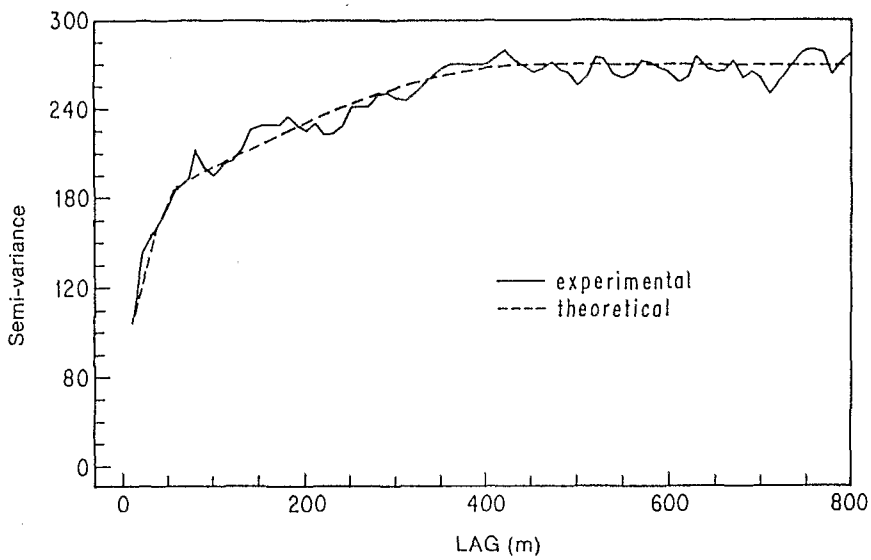

Figure 8. Experimental semi-variogram obtained from airborne SPOT simulation data (channel XS2) and theoretical double spherical model.

structures of albedo and surface temperature appear different but persistent through time. From high resolution data, experimental semi-variograms suggest the existence of multiple structures of varying size. A theoretical model of nested environmental variables influencing spectral response has been proposed, which could explain variability in remotely-sensed data observed at several scales.

Table 4. Idealized geometric progression of ranges of environmental variables influencing remotely-sensed measurements.

Variable	Range (m)	Validation data
Radiation absorbed by the canopy	4	Hemispherical photographs radiation measurements under the canopy, mean diameter of tree crowns
Soil water content	40	Neutron probe transections airborne microwave data
Orotopography	400	Digital terrain model airborne data or high resolution satellite data: radiance, brightness index
Vegetation physiognomy, landscape unit	4000	High resolution satellite data: vegetation index
Climatic variables actual evapotranspiration	40000	Low resolution satellite data: thermal infrared, visible, near-infrared

References

BURROUGH, P. A., 1983, Multiscale sources of spatial variation in soil. I. The application of fractal concepts to nested levels of soil variation. *Journal of Soil Science*, **34**, 577-597.

CLARK, I., 1979, *Practical Geostatistics* (London: Applied Science Publishers).

COHEN, W. B., SPIES, T. A., and BRADSHAW, G. A., 1990, Semivariograms of digital imagery for analysis of conifer canopy structure. *Remote Sensing of Environment*, **34**, 167-178.

CRESSIE, N., 1985, Fitting variogram models by weighted least squares. *Mathematical Geology*, **17**, 563-586.

CURRAN, P. J., 1988, The Semivariogram in Remote Sensing: an introduction. *Remote Sensing of Environment*, **24**, 493-507.

DECOLA, L., 1989, Fractal analysis of a classified Landsat scene. *Photogrammetric Engineering and Remote Sensing*, **55**, 601-610.

GRAETZ, R. D., 1990, Remote sensing of ecosystem structure: an ecologist's pragmatic view. In *Remote Sensing of Biosphere Functioning*, edited by R. J. Hobbs and H. A. Mooney (New York: Springer Verlag), pp. 5-30.

JONES, J. G., THOMAS, R. W., and EARWICKER, P. G., 1991, Multiresolution analysis of remotely sensed imagery. *International Journal of Remote Sensing*, **12**, 107-124.

LACAZE, B., DEBUSSCHE, G., JARDEL, J., 1984, Analyse de l'hétérogénéité spatiale d'un taillis de Chêne vert (*Quercus ilex* L.) à l'aide de techniques visuelles, photographiques et radiométriques. *Actes du 2ème Colloque international Signatures spectrales d'objets en télédétection*, Les Colloques de l'INRA No. 23 (Paris: INRA Publ.), pp. 265-275.

LACAZE, B., LAHRAOUI, L., DEBUSSCHE, G., and KHELFA, A., 1985, Analyse de mesures radiométriques de simulation SPOT en milieux méditerranéens aride et subhumide. *Proceedings of the 3rd International Colloquium on Spectral Signatures in Remote Sensing*, ESA/SP-147 (Noordwijk, The Netherlands: ESA Publications Division), pp. 425-428.

MANDELBROT, B., 1975, *Les objets fractals. Forme, hasard et dimension* (Paris: Flammarion).

MATHERON, G., 1965, *Les variables régionalisées et leur estimation* (Paris: Masson).

MERIAUX, S., ROLLIN, H., and RUTTEN, P., 1979, Effets de la sécheresse sur la vigne. I. Etudes sur Cabernet-Sauvignon. *Annales agronomiques*, **30**, 553-575.

NATIONAL AERONAUTICS AND SPACE ADMINISTRATION (NASA), 1980, *Heat Capacity Mapping mission. User's Guide*. Second revision (Greenbelt, Maryland: Goddard Space Flight Center).

PALMER, M. W., 1988, Fractal geometry: a tool for describing spatial patterns of plant communities. *Vegetatio*, **75**, 91-102.

RAMBAL, S., LACAZE, B., and WINKEL, T., 1990, Testing an area-weighted model for albedo or surface temperature of mixed pixels in Mediterranean woodlands. *International Journal of Remote Sensing*, **11**, 1495-1499.

RAMSTEIN, G., and RAFFY, M., 1989, Analysis of the structure of radiometric remotely-sensed images. *International Journal of Remote Sensing*, **10**, 1049-1073.

REINIGER, P., 1981, HCMM Satellite data calibration and atmospheric corrections. *Tellus Newsletter*, **25**, 1-16.

ROWE, J. S., 1961, The level-of-integration concept and ecology. *Ecology*, **42**, 420-427.

SURRA, J., 1968, Les structures gigognes: morphologie mathématique et interprétation métallogénique. *Mineralium Deposita*, **3**, 135-154.

TRANGMAR, B. B., YOST, R. S., and UEHARA, G., 1985, Application of geostatistics to spatial studies of soil properties. *Advances in Agronomy*, **38**, 45-94.

WEBSTER, R., 1985, Quantitative analysis of soil in the field. *Advances in Soil Science*, **3**, 1-70.

WOODCOCK, C. E., STRAHLER, A. H., and JUPP, D. L. B., 1988, The use of variograms in remote sensing. II: Real digital images. *Remote Sensing of Environment*, **25**, 349-379.